X-Disciplinarity

DOI: https://doi.org/10.63174/xdi.LHDR8582

Original Article

Electrolyte Density Detection using Plasma-Modified FP Cavity Sensor for Lead-Acid Battery Health Management

https://doi.org/10.63174/xdi.LHDR8582

Volume 2 Issue 1

Received: 16 Mar 2026

Accepted: 17 Mar 2026

Published: 18 Mar 2026

Open Access

Ruiting Li[1], Faqian Liu[1], Mengchao Gao[1], Duo Chen[1,*], Hao Mi[1], Zhen Zhang[1]

Abstract: In-situ density monitoring of lead-acid battery electrolytes faces challenges from bubble adhesion, turbidity, and high temperatures. This study presents a fiber optic Fabry-Perot (FP) sensor featuring an oxygen plasma-modified superhydrophilic probe encased in a 300-mesh nylon package. The superhydrophilic surface prevents bubble adhesion by promoting rapid liquid spreading, while the nylon mesh filters suspended impurities and mitigates hydrodynamic turbulence. Experimental results demonstrate excellent stability over 19 days at 45°C, with fluctuations ≤0.005 g/cm³. Under conditions of vigorous bubble evolution and impurity stirring, the composite design reduces measurement error from >0.05 g/cm³ to <0.01 g/cm³. This robust sensing scheme offers a reliable solution for the life-cycle health management of lead-acid batteries.

1. Introduction

Lead-acid batteries, with their advantages of low cost, mature technology, and high safety, occupy an irreplaceable position in Uninterruptible Power Supply (UPS), automotive Starting-Lighting-Ignition (SLI) systems, and large-scale energy storage fields [1-3]. Real-time monitoring of the State of Health (SOH) is crucial for ensuring the safe operation of energy storage systems [4]. As a key parameter of the electrolyte, the density of the sulfuric acid solution directly reflects the State of Charge (SOC) and aging degree of the battery [5]. Typically, the electrolyte density varies from approximately 1.10 to 1.30 g/cm³ during a full charge-discharge cycle. However, traditional electrolyte density measurement methods, such as the hydrometer method and Archimedes buoyancy method, are typically bulky, cumbersome to operate, and difficult to integrate into the battery for in-situ online monitoring [6, 7]. In recent years, optical fiber sensors have become a research hotspot for internal battery environment monitoring due to their small size, immunity to electromagnetic interference, corrosion resistance, and intrinsic safety [8, 9]. Among them, optical fiber sensors based on the Fabry-Perot (FP) interference principle exhibit extremely high measurement sensitivity by utilizing the correspondence between liquid refractive index and density [10-12].

Although fiber optic FP sensors perform excellently in laboratory environments, their long-term stability and reliability face severe challenges under the actual operating conditions of lead-acid batteries. First is the bubble interference problem; vigorous hydrogen and oxygen evolution reactions occur during the late stages of charging and overcharging [13]. Microbubbles easily adhere to the hydrophobic optical fiber end face, causing light scattering or sudden refractive index changes within the FP cavity, leading to severe signal fluctuations or even measurement failure [14, 15]. Second is the complex solid-liquid multiphase flow environment. As the battery ages, electrode active materials (such as lead dioxide and lead sulfate particles) detach and suspend in the electrolyte, forming a turbid system [16]. These suspended impurities frequently impact the sensor surface under thermal convection or stirring, causing severe signal noise. Furthermore, the internal temperature can rise above 45°C during high-current operation, placing higher demands on the temperature resistance and long-term chemical stability of the sensing materials [17].

To address the above issues, existing research has mostly focused on inhibiting bubble adhesion through physical structural design or chemical coatings [18]. However, single surface modification is difficult to simultaneously cope with the dual interference of “bubble adhesion” and “impurity impact.” For example, while superhydrophilic coatings can effectively release bubbles, they are prone to failure due to mechanical wear in turbulent environments containing suspended particles [19]; conversely, simple physical packaging can block impurities but often leads to bubble accumulation due to poor exhaust, forming a new source of interference [20]. Therefore, developing a sensor structure that can withstand high-temperature acidic environments while simultaneously resisting bubble and impurity interference is key to realizing in-situ monitoring of lead-acid batteries.

This study proposes an anti-interference fiber optic FP electrolyte density sensor designed for the complex operating conditions of lead-acid batteries. First, based on oxygen plasma surface modification technology, a superhydrophilic micro-nano structure is constructed at the quartz sensing interface to fundamentally reduce the adhesion of bubbles on the probe surface. Second, a 300-mesh nylon mesh flexible packaging structure is innovatively introduced, utilizing its microporous sieving effect to block suspended impurities and turbulent impact in the electrolyte while maintaining free permeation of the electrolyte. Finally, a comprehensive test system simulating battery operating conditions was built to systematically evaluate the long-term stability of the sensor under high temperature (45°C), bubble evolution, and impurity disturbance conditions. Experimental results show that the composite structure sensor operates continuously for 19 days in a 45°C high-temperature acidic environment with density measurement fluctuations below 0.005 g/cm³ and maintains signal stability under severe bubble and impurity interference, providing a reliable sensing solution for the intelligent operation and maintenance of lead-acid batteries throughout their life cycle.

[1] China-Belarus Belt and Road Joint Laboratory on Intelligent Perception in Extreme Environments, Shandong Key Laboratory of Optoelectronic Sensing Technologies, International School for Optoelectronic Engineering, Qilu University of Technology (Shandong Academy of Sciences), Jinan, China

[*] Corresponding author: sdkdcd@163.com

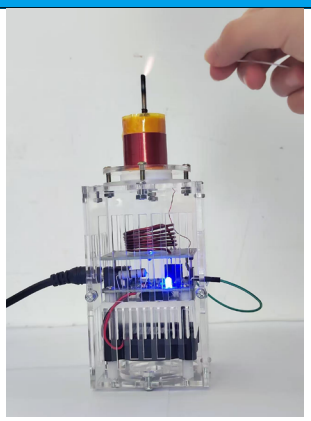

Figure 1. Self-made high-voltage micro-arc oxygen plasma treatment device

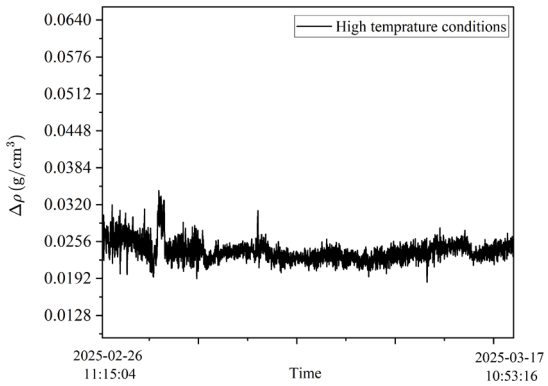

Figure 2. Long-term stability test curve of the sensor in a 45°C high-temperature acidic environment (19 days).

2. Sensor Design and Fabrication

2.1. Sensor Working Principle and Signal Demodulation Strategy

This study employs the optical fiber Fabry-Perot (FP) interference principle for electrolyte density detection. The sensor probe consists of a single-mode fiber end face and a reflective surface forming a low-finesse FP cavity. When light from a broadband source is transmitted to the sensor head, part of the light undergoes Fresnel reflection (R_1) at the fiber-air/liquid interface, and the remaining light is transmitted and undergoes secondary reflection (R_2) at the reflective surface. The two reflected beams return along the original path and interfere [21].

The light intensity of the interference spectrum $I(\lambda)$ can be expressed as:

$$I(\lambda) = I_1 + I_2 + 2\sqrt{I_1 I_2}\cos\left(\frac{4\pi nL}{\lambda} + \phi_0\right) \quad (1)$$

where I_1 and I_2 are the intensities of the two reflected beams, λ is the incident light wavelength, L is the FP cavity length, n is the refractive index of the medium inside the cavity (electrolyte), and $\phi_0$is the initial phase. For sulfuric acid electrolyte, there is a significant linear positive correlation between its density ρ and refractive index n (an approximation of the Lorentz-Lorenz relation) [22]. The optical path difference (OPD = $2nL$) of the FP cavity was demodulated using the Fast Fourier Transform (FFT) method or Peak Tracking method. Since the physical cavity length L remains constant, by demodulating the OPD change of the interference spectrum, the refractive index of the electrolyte can be retrieved, and its density value can be accurately calculated.

It is worth noting that although the core measurement parameter (electrolyte density) relies on the demodulation of the intra-cavity phase, the light intensity characteristics of the interference spectrum (such as average reflected light intensity and fringe visibility) play a key auxiliary diagnostic role in anti-interference monitoring under complex conditions. When microbubbles adhere to the fiber end face, since the refractive index difference between air ($n \approx 1.0$) and quartz ($n \approx 1.45$) is much larger than that between the electrolyte and quartz, the interface reflectivity increases dramatically, manifesting as an abnormal mutation in the light intensity signal on the demodulator. Conversely, when the electrolyte generates suspended impurities due to aging, the scattering effect of particles causes attenuation of the return light energy and a decrease in Fringe Visibility. Therefore, this system not only demodulates cavity length data but also synchronously monitors the time-domain evolution of light intensity characteristics to identify failure modes such as bubble blocking and impurity deposition in real-time, providing an important basis for evaluating the robustness of the sensor.

2.2. Hydrophilic Modification of Sensor Surface

In the late stages of lead-acid battery charging and discharging, vigorous hydrogen and oxygen evolution reactions occur on the electrode surface. Due to the inherent hydrophobicity of the standard quartz fiber surface, microbubbles easily adhere to the sensor end face, causing sudden changes in the refractive index at the gas-liquid interface, resulting in long-term signal drift or measurement dead-locking.

To solve this problem, this study introduces Oxygen Plasma surface treatment technology. The experiment uses a self-made high-voltage micro-arc plasma generator (as shown in **Figure 1**), which consists of a high-voltage power supply, a boost coil, and a needle tip discharge electrode.

Excited by a high-voltage electric field, oxygen molecules in the air are ionized to form a highly active oxygen plasma stream. The cleaned FP sensor probe is placed in the plasma flame flow for 30~60 seconds. High-energy particles bombard the quartz (SiO_2) surface, breaking the original siloxane bonds (Si-O-Si) and combining with moisture in the environment to form polar silanol groups (Si-OH) [23]. This process significantly increases the surface energy of the fiber surface, transforming it from a hydrophobic to a superhydrophilic state (contact angle < 5°). When bubbles contact the modified surface, the electrolyte rapidly spreads on the sensor surface under surface tension to form a water film, forcing the bubbles to slide off quickly. The superhydrophilic characteristic at the physical level is reflected in the optical signal, manifesting as the conversion of bubble-induced interference light intensity perturbations from “long-term baseline drift” in the untreated state to “high-frequency, extremely low-amplitude transient pulses,” thereby ensuring the continuity and accuracy of density demodulation [24].

2.3. Design of Anti-Impurity Composite Packaging Structure

Although hydrophilic modification effectively solves the bubble adsorption problem, tests in simulated turbid electrolytes of aged batteries revealed that simple bare probes are highly susceptible to mechanical impact from suspended particles (such as detached active material PbO_2 or graphene microparticles), leading to sudden drops in light intensity and significantly increased signal noise floors. Furthermore, continuous particle scouring may also lead to long-term mechanical wear of the hydrophilic coating.

To this end, this study designed a multi-level protective packaging structure oriented towards complex multiphase flow environments:

Rigid Support Layer: A rigid shell with liquid-permeable holes is fabricated using acid-resistant polymer material to protect the internal fragile quartz fiber probe from direct physical collision with large particles.

Flexible Filter Mesh Layer: Targeting micron-level suspended impurities, a layer of 300-mesh (approximately 48 μm pore size) nylon filter mesh is wrapped around the outside of the rigid shell. This pore size was optimized to effectively block the vast majority of suspended electrolyte particles and turbulence impact generated by magnetic stirring, while ensuring free capillary permeation of the sulfuric acid solution inside the sensor to ensure real-time balance of internal and external liquid densities [25].

This “inner superhydrophilic probe + outer nylon filter mesh” composite structure utilizes the microporous sieving effect of the nylon mesh to block external solid-phase impurities, while simultaneously utilizing the internal superhydrophilic interface to prevent the retention and accumulation of infiltrated microbubbles, achieving effective immunity to the “bubble-impurity” gas-solid dual-phase interference in lead-acid batteries.

3. Results and Discussion

3.1. Temperature Stability and Long-term Drift Characteristics

The internal temperature of lead-acid batteries often rises significantly (up to 45°C or more) during rapid charging/discharging or high-current operation. Therefore, the long-term baseline stability of the sensor in a high-temperature acidic environment is the primary indicator for evaluating its suitability for

in-situ monitoring. In this experiment, the packaged fiber optic FP sensor was placed in a constant temperature water bath acidic solution at 45°C for continuous monitoring over 19 days.

As shown in **Figure 2**, during the 19-day continuous high-temperature operation, the density conversion value demodulated by the sensor exhibited extremely high stability, with baseline fluctuation amplitude strictly controlled within the range of ≤0.005 g/cm³ for the vast majority of the time. The transient fluctuations observed were correlated with the replenishment of the water bath to compensate for evaporation. These external environmental disturbances are distinct from the sensor's intrinsic drift and can be easily identified and filtered in practical applications. This result fully demonstrates the excellent durability of the quartz fiber material and the acid-resistant polymer packaging structure designed in this paper under high-temperature strong acid environments. As a comparison, in a long-cycle test at a low temperature of 20°C (data not shown), the sensor showed slight signal drift after 12 days of operation, which may be related to stress relaxation of the polymer packaging material or electrolyte stratification at low temperatures. Overall, the sensor possesses the capability to work stably for long periods under battery high-temperature heating conditions. It is worth noting that while plasma-treated surfaces typically undergo hydrophobic recovery in air, continuous immersion in the aqueous electrolyte solution helps stabilize the surface silanol groups (Si-OH). Our post-experiment measurements showed that after 19 days of immersion, the contact angle of the probe surface increased slightly from <5° to approximately 15°, which is still sufficient to maintain the superhydrophilic state and effectively prevent bubble adhesion.

3.2. Performance Evaluation under Bubble Interference

To verify the suppression effect of plasma hydrophilic modification on bubble interference, a DC water electrolysis device (voltage set to 4~6V) was built to simulate the hydrogen and oxygen evolution reactions in the late stage of lead-acid batteries. An untreated bare sensor and an oxygen plasma hydrophilically treated sensor were placed above the electrodes, directly exposing them to a dense stream of microbubbles.

Figure 3(a) intuitively demonstrates the destructive impact of bubbles on measurement. The untreated sensor, influenced by the hydrophobic interface, easily suffered from large bubble signal stagnation at its end face, causing the optical path to be blocked by the air interface and leading to severe irregular signal jumps. In contrast, the sensor treated with oxygen plasma (No. 11) exhibited excellent anti-interference ability, with a highly stable data curve. Local magnification analysis of this curve (**Figure 3b**) shows that the difference between the maximum and minimum fluctuation values is only 0.069 g/cm³ ~ 0.078 g/cm³. This indicates that the superhydrophilic interface prompts the electrolyte to spread rapidly on the probe surface, allowing microbubbles to only slide briefly over the surface rather than staying and accumulating for a long time. This rapid physical detachment transforms the optical signal disturbance from "low-frequency, large-amplitude" baseline drift to "high-frequency, extremely low-amplitude" transient pulses, thereby ensuring the validity of the density measurement.

3.3. Impurity Turbulence Environment and Optimization of

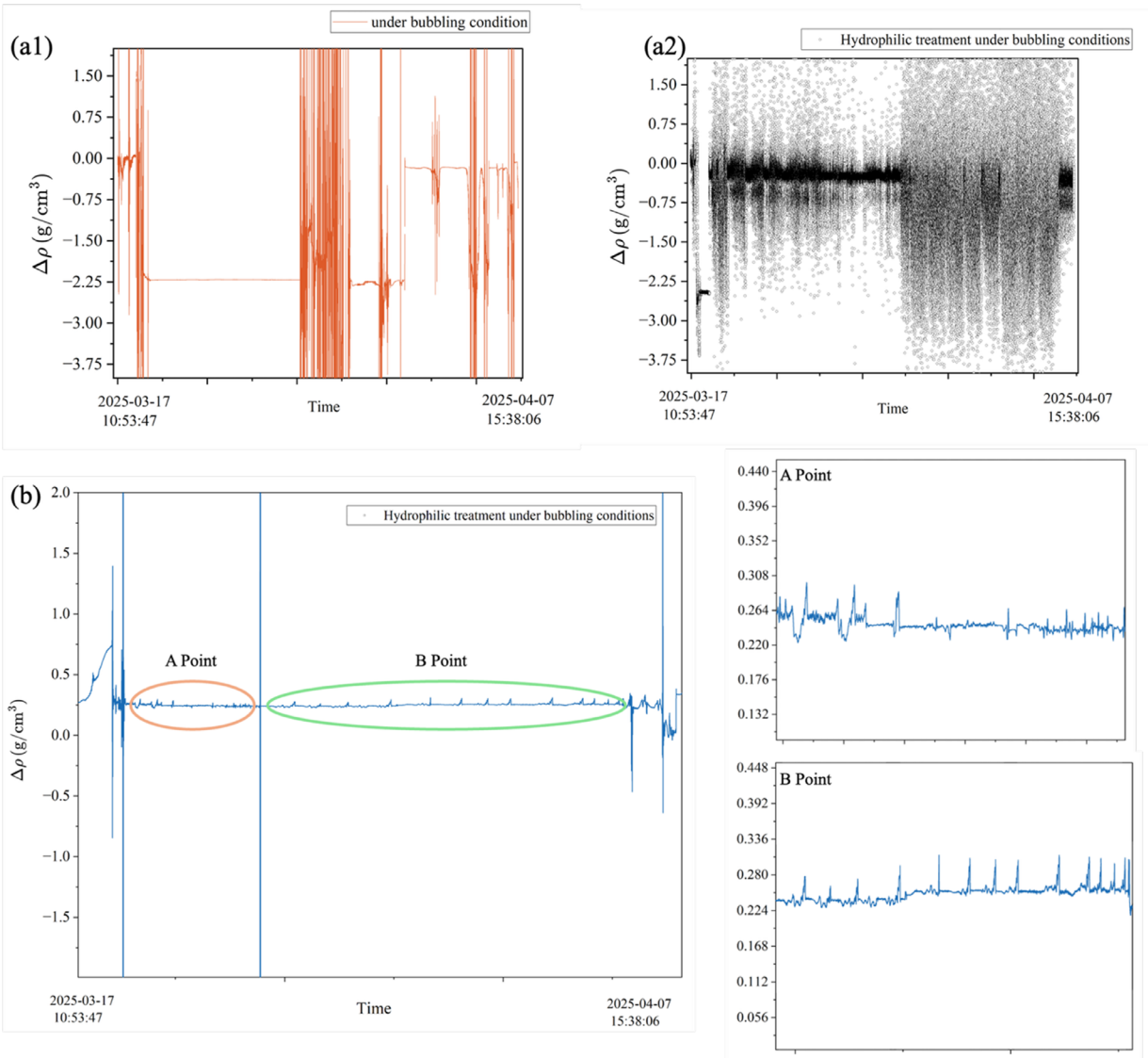

Figure 3. **Sensor response under bubble interference conditions.** (a) Global comparison of density fluctuations for sensors with different treatments; (b) Local magnified signal of the hydrophilic modified sensor (No. 11).

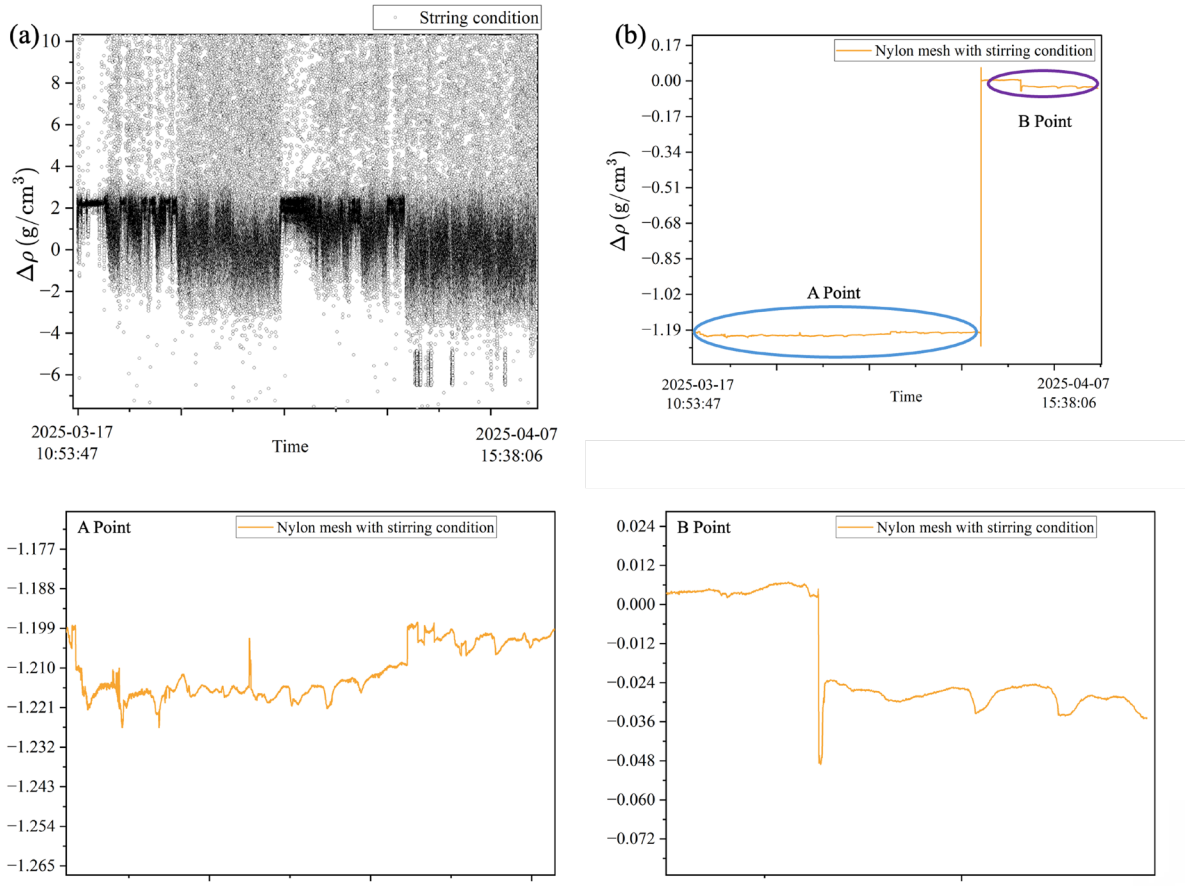

Figure 4. **Measurement comparison under impurity and turbulence interference.** (a) Severe fluctuation of the bare sensor; (b) Stable output of the sensor with 300-mesh nylon net composite packaging.

Composite Packaging Structure

In addition to bubbles, the turbid multiphase flow formed by detached active materials (such as PbO_2 particles) suspended in the electrolyte of aged batteries under thermal convection is another major source of interference. To this end, the experiment utilized a magnetic stirrer and added lead powder/graphite microparticles to simulate a severe impurity turbulence environment.

As shown in **Figure 4(a)**, under impurity stirring conditions, the bare sensor exhibited substantial errors of >0.05 g/cm³ every minute. More seriously, the experiment found that the simple hydrophilic coating failed after a brief period of stability of about 30 minutes. This is mainly because the turbulence generated by magnetic stirring carries high-hardness particulate matter that continuously scours and impacts the sensor surface, causing the micro-nano hydrophilic structure to be destroyed under mechanical wear.

Addressing the critical challenge of "coating non-wear-resistance," this paper introduced a physical filter packaging of "shell + 300-mesh nylon mesh." As shown in **Figure 4(b)**, the sensor wrapped with nylon mesh successfully isolated the physical impact of particulate matter and fluid drag interference. In continuous stirring tests lasting tens of hours, the locally magnified fluctuation extreme difference was only 0.011 g/cm³ ~ 0.027 g/cm³. The data indicates that the microporous filter mesh structure effectively functions as an anti-fouling barrier while allowing free ion diffusion (ensuring density balance).

3.4. Comprehensive Verification in Simulated Real Conditions and the Bubble-Impurity Trade-off Mechanism

In the real aging process of lead-acid batteries, bubbles and impurities are often concomitant. In a 72-hour continuous graphite rod electrolysis experiment, the electrolyte gradually turned from transparent to brownish-black (simulating massive detachment and peeling of active materials), accompanied by continuous bubble generation.

Under comprehensive conditions of extreme turbidity and rich bubbles, the "inner superhydrophilic + outer nylon mesh" composite structure proposed in this study demonstrated good trade-off performance: the nylon mesh effectively prevented black suspended matter from contaminating the optical end face, ensuring no signal loss occurred even after the solution turned completely black.

However, the experiment also revealed a trade-off mechanism: the porosity of the nylon mesh is positively correlated with the retention rate of bubbles. Due to the lack of a dynamic surface renewal mechanism, extremely small bubbles generated in the solution, after passing through the nylon mesh, tend to gradually accumulate and merge into large bubbles within the mesh enclosure space, thereby slowly pushing up the measurement baseline. As shown in **Figure 5,** when manual vacuum pumping was used to exhaust the accumulated bubbles inside the mesh, the signal fluctuation rapidly converged to the high-precision range of 0.008~0.049 g/cm³. It should be noted that manual pumping is primarily for laboratory validation of the mechanism, whereas practical field applications will require passive exhaust designs.

This phenomenon indicates that the current composite packaging structure can solve most static interferences. However, under extreme boiling gas evolution conditions, the exhaust mechanism within the mesh still needs optimization. Future research will consider introducing an asymmetric composite structure of "rigid support large-pore titanium mesh + flexible hydrophobic breathable membrane" to achieve unidirectional autonomous discharge of internal bubbles while blocking impurities.

Although manual vacuum pumping was used in this static laboratory setup to remove accumulated bubbles,in practical engineering applications, this issue can be mitigated by optimizing the installation orientation. By installing the sensor vertically with the probe tip facing downwards, the buoyancy of larger aggregated bubbles will facilitate their natural upward escape from the mesh. Additionally, the inevitable vibration in operational environments (e.g., automotive batteries) will further assist in detaching bubbles from the nylon mesh, eliminating the need for manual intervention.

Since the refractive index and density of the sulfuric acid electrolyte are temperature-dependent, a comprehensive monitoring system would integrate a separate temperature sensor (such as a Fiber Bragg Grating or thermocouple)

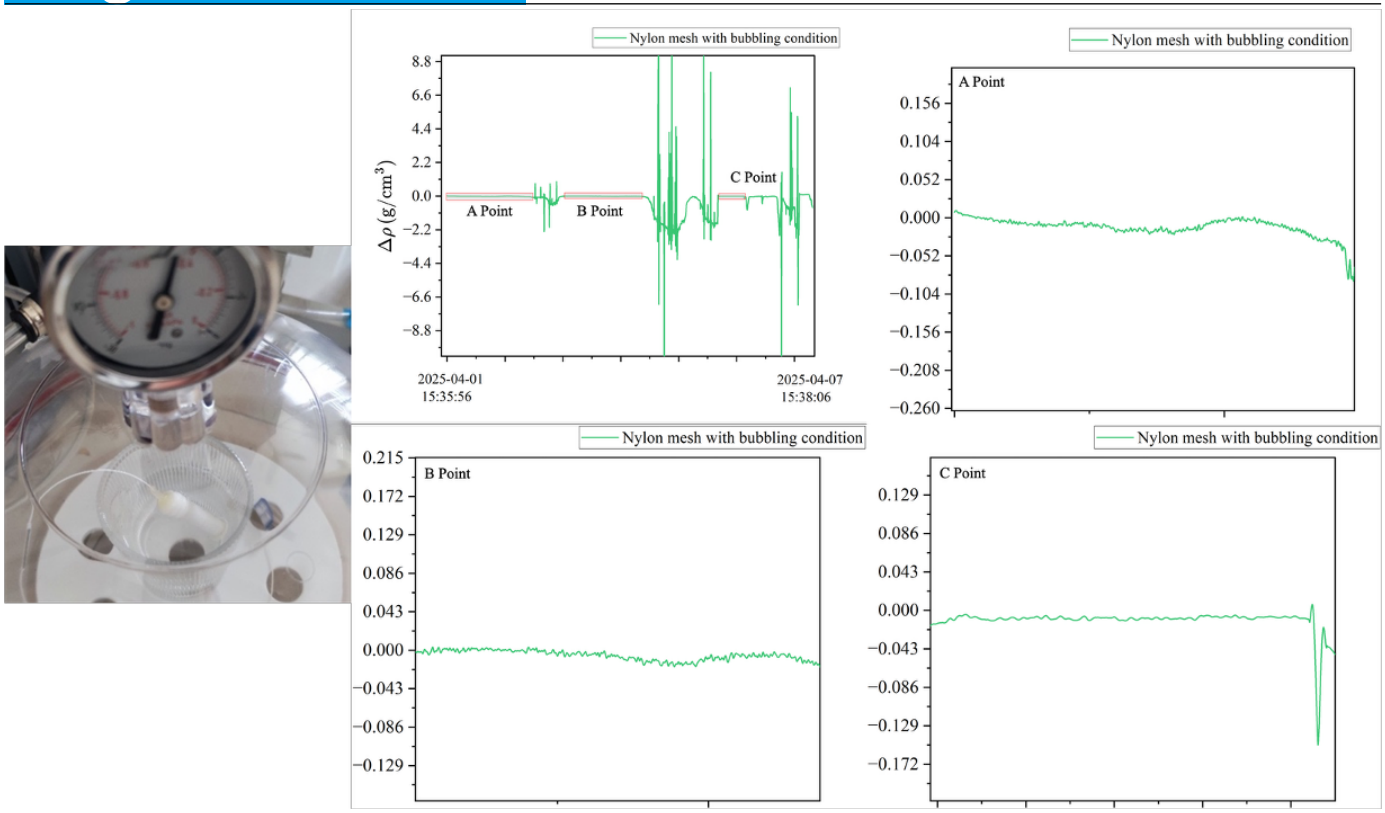

Figure 5. Bubble accumulation phenomenon in extremely turbid electrolyte and signal recovery after vacuum exhaust.

alongside the FP density sensor. The final density value can be accurately calculated by compensating for temperature fluctuations using the standard thermo-optic coefficient of the sulfuric acid solution.

4. Conclusion

This study addressed the multiple interference problems such as high temperature, bubble adhesion, and impurity turbulence faced in the in-situ monitoring of lead-acid battery electrolyte density by proposing a fiber optic FP cavity sensor scheme based on the synergy of "oxygen plasma superhydrophilic modification" and "flexible nylon filter mesh packaging." Experimental results show that the sensor operated continuously for 19 days in a 45°C high-temperature acidic environment, with density measurement fluctuations consistently maintained within the range of ≤0.005 g/cm³, demonstrating excellent thermal stability and chemical durability. Oxygen plasma treatment significantly improved the wettability of the probe surface, effectively inhibiting the bubble dead-locking phenomenon and transforming large signal drifts into high-frequency micro-perturbations. Meanwhile, the 300-mesh nylon mesh packaging structure successfully blocked the mechanical impact and abrasion of the probe by suspended particles, reducing the measurement error to within 0.01 g/cm³ under impurity turbulence conditions. Although comprehensive tests revealed that the physical filter mesh may lead to the accumulation of microbubbles while blocking impurities, which requires further optimization through vacuum pumping or future improvements in breathable membrane structures, overall, the composite anti-interference sensing scheme proposed in this study effectively solves the signal distortion problem in harsh environments, providing important theoretical basis and technical support for the hardware development of the next-generation lead-acid battery full life cycle State of Health (SOH) management system.

Author Contributions

L.R.T. conceived the research idea and designed the study; L.F.Q. performed the experiments and data collection; G.M.C. analyzed and processed the experimental data; M.H. and Z.Z. assisted in the experiment and revised the manuscript; D.C. supervised the entire research process, provided funding support, and revised and finalized the manuscript. All authors have read and approved the final manuscript.

Funding

Shandong Provincial Natural Science Foundation (ZR2022QF083); Taishan Scholar Youth Expert Program (tsqn202306254); Talent Introduction Program of Qilu University of Technology (2023RCKY033); Jinan Higher Education Innovation Project (2023GXRC062): Optical Fiber Sensing Technology for Oil and Gas Well Monitoring (Project Funding: 300,000 RMB, Implementation Period: 2024–2026)

Conflicts of Interest

The authors declare that the research was conducted in the absence of any commercial or financial relationships that could be construed as a potential conflict of interest.

References

[1] G. J. May, A. Davidson, B. Monahov. "Lead batteries for utility energy storage: a review." *J. Energy Storage* **2018**, *15*, 145–57.
[2] S. Jiang, Z. Song. "A review on the state of health estimation methods of lead-acid batteries." *J. Power Sources* **2022**, *517*, 230710.
[3] D. E. O. Juanico. "Revitalizing lead-acid battery technology: a comprehensive review on material and operation-based interventions with a novel sound-assisted charging method." *Front. Batter. Electrochem.* **2024**, *2*, 1–19.
[4] S. M. M. Alavi, C. R. Birkl, D. A. Howey. "Time-domain fitting of battery electrochemical impedance models." *J. Power Sources* **2015**, *288*, 345–52.
[5] C. Piat, A. Sari, C. Viton. "Emerging battery technologies: the main aging mechanisms and challenges." *Batteries* **2025**, *11*, 10, 383–424.
[6] J. Huang, L. Albero Blanquer, J. Bonefacino, E. R. Logan, D. Alves Dalla Corte, C. Delacourt, B. M. Gallant, S. T. Boles, J. R. Dahn, H.-Y. Tam, J.-M. Tarascon. "Operando decoding of chemical and thermal events in commercial Na(Li)-ion cells via optical sensors." *Nat. Energy* **2020**, *5*, 9, 674–83.
[7] J. M. Leça, Y. Magalhães, P. Antunes, V. Pereira, M. S. Ferreira. "Real-time measurement of refractive index using 3D-printed optofluidic fiber sensor." *Sens.* **2022**, *22*, 23, 9377.
[8] D. Duan, J. Yang, Y. Tang, Y.-Y. Xie. "Diamond-based fiber-optic fabry–perot interferometer with ultrawide refractive-index measurement range." *Photonics* **2024**, *11*, 8, 763.
[9] X. Xue, X. Han, W. Li, K. Li, F. Liu, T. Guo. "Operando battery

monitoring: lab-on-fiber electrochemical sensing technologies." *Laser Photonics Rev.* **2024**, *18*, 9, 2301298.
[10] K. Kaushal, B. Das. "Polymer transduction cavity based optical fiber fabry-perot interferometer for VOC sensing." *Results Opt.* **2023**, *12*, 100479.
[11] J. Leça, Y. Magalhães, P. Antunes, V. Pereira, M. Ferreira. "Optofluidic fabry-perot interferometric sensor for the real-time measurement of refractive index." *J. Phys. Conf. Ser.* **2022**, *2407*, 1, 012021.
[12] S. Cao, X. Shang, H. Yu, L. Shi, L. Zhang, N. Wang, M. Qiu. "Two-photon direct laser writing of micro fabry-perot cavity on single-mode fiber for refractive index sensing." *Opt. Express* **2022**, *30*, 14, 25536–43.
[13] E. Lemaire, L. Serra, C. Arnal, F. Ardiaca, D. Monchal, N. Guillet, A. Kirchev. "Study of the operation of lead–acid battery electrodes under hybrid battery–electrolyzer cycling profiles." *Batteries* **2025**, *11*, 4, 137.
[14] K. Malysa, M. Krasowska, M. Krzan. "Influence of surface active substances on bubble motion and collision with various interfaces." *Adv. Colloid Interface Sci.* **2005**, *114–115*, 205–25.
[15] C. Diaz, A. Leal Junior, C. A. F. Marques, A. Frizera, M. Pontes, P. Antunes, P. Andre, M. R. N. Ribeiro. "Optical fiber sensing for sub-millimeter liquid-level monitoring: a review." *IEEE Sensors J.* **2019**, *PP*, 1–1.
[16] E. Lemaire, L. Serra, C. Arnal, F. Ardiaca, D. Monchal, N. Guillet, A. Kirchev. "Study of the operation of lead–acid battery electrodes under hybrid battery–electrolyzer cycling profiles." *Batteries* **2025**, *11*, 4, 137.
[17] S. J. Mihailov. "Fiber bragg grating sensors for harsh environments." *Sens.* **2012**, *12*, 2, 1898–918.
[18] J. Yong, F. Chen, Y. Fang, J. Huo, Q. Yang, J. Zhang, H. Bian, X. Hou. "Bioinspired design of underwater superaerophobic and superaerophilic surfaces by femtosecond laser ablation for anti- or capturing bubbles." *ACS Appl. Mater. Interfaces* **2017**, *9*, 45, 39863–71.
[19] I. S. Bayer. "On the durability and wear resistance of transparent superhydrophobic coatings." *Coatings* **2017**, *7*, 1, 12.
[20] X. Zhu, Z. Zhang, X. Men, J. Yang, K. Wang, X. Xu, X. Zhou, Q. Xue. "Robust superhydrophobic surfaces with mechanical durability and easy repairability." *J. Mater. Chem.* **2011**, *21*, 39, 15793–97.
[21] B. H. Lee, Y. H. Kim, K. S. Park, J. B. Eom, M. J. Kim, B. S. Rho, H. Y. Choi. "Interferometric fiber optic sensors." *Sens.* **2012**, *12*, 3, 2467–86.
[22] C.-Y. Tan, Y.-X. Huang. "Dependence of refractive index on concentration and temperature in electrolyte solution, polar solution, nonpolar solution, and protein solution." *J. Chem. Eng. Data* **2015**, *60*, 10, 2827–33.
[23] V. Jokinen, P. Suvanto, S. Franssila. "Oxygen and nitrogen plasma hydrophilization and hydrophobic recovery of polymers." *Biomicrofluidics* **2012**, *6*, 1, 016501-016501–10.
[24] X. Shi, Z. Zhang, F. Tao, H. Ji, X. Ji, Z. Tian, J. Chen. "Hydrophilic modification of cellulose using sulfamic acid for optical fiber humidity sensor fabrication." *Cellulose* **2023**, *30*, 5, 3113–25.
[25] M. Palencia, J. M. Martínez-Lara, J. M. Durango, J. S. L. Vélez, E. M. Combatt. "A simple method for porous structure characterization of ultrafiltration membranes from permeability data and hydrodynamic models: a semi-empirical approach." *Surfaces* **2026**, *9*, 1, 5.